

# Rehabilitation and Strengthening of Rectangular Hollow Section Steel Beams Using Carbon Fiber Reinforced Polymer

Wael A. Salah

Civil Engineering Department, Al-Azhar University/Faculty of Engineering, Cairo, Egypt

## ABSTRACT

This paper presents the behavior of cracked rectangular hollow section (RHS) steel beams retrofitted using carbon fiber reinforced polymer (CFRP) plate. The finite element (FE) analysis is employed to investigate the behavior of initially cracked RHS steel beams. A three dimensional (3D) FE model is developed using ABAQUS software to analyze and investigate the initially cracked RHS steel beams. The results of the FE are validated through the comparisons with the acquired literature experimental results. Then a sort of parametric studies is conducted to investigate the effect of certain parameters of the adhesive material on the strength of the rehabilitated RHS steel beams.

**Keywords:** CFRP, RHS, Steel beam, Finite Element, Analysis, Strengthening, adhesive

## I. INTRODUCTION

Hollow steel sections have been employed in a large scale in many steel structures due to their efficient bearing loads. Several existing steel structures suffering from the deficient loading bearing capacity owing to many reasons as corrosion, cracks, and unexpected increasing in the imposed loads. Carbon Fiber Reinforced Polymer (CFRP) composite plates have been widely utilized in strengthening and retrofitting both of concrete and steel structures. Superior physical properties of such composite laminates have encouraged numerous researchers to recommend them in retrofitting and strengthening of various steel or concrete structural elements.

Recently, the number of studies concerning the use of CFRP in strengthening and repairing of steel structures has been significantly increased. The major number of these studies have been directed to investigate the effect of CFRP strengthening of I-shaped steel beams [1], [2]. While Steel I-beams with web openings strengthened with CFRP laminates, have been analyzed by Mohammed et al. [3] to evaluate the recoverable strength could be attained using such kind of strengthening approach. On the other hand, cold-formed thin-walled channel beams were strengthened with

transverse CFRP interval strips around web and flanges and were exposed to eccentric compression load as presented by Hongyuan et al. [4].

Less attention has been intended for the steel elements of hollow section strengthened using CFRP. Very high strength circular steel tubes have been strengthened using various lap shear patches of CFRP which utilized in that study as a butt-weld material by joining two circular tube elements side-by-side [5]. The circular tube specimens, were exposed to axial tension force exhibited a meaningful growing in the ultimate strength using such kind of CFRP strengthening technique. While strengthening of very high strength circular steel tubes subjected to axial load, using a high modulus of CFRP, has shown an augment in the tensile capacity [6]. The performance of steel beams and short column of circular cross section strengthened with CFRP laminates has been explored by Haedir J. and Zhao X. L. [7]. An analytical model for estimating the ultimate moment capacity of steel circular tube beams strengthened with CFRP has been introduced. A sort of experimental programs, has been conducted by Shanmugavalli B. and Sundarraja M.C. [8] to study the effect of CFRP strengthening a circular hollow section steel column exposed to axial compression loads. The carried-out tests resulted in the confinement of circular steel

columns with CFRP, significantly improved both of the column load carrying capacity and axial deformations.

Xiao-Ling Zhao et al. [9] have evaluated the web crippling behavior of RHS strengthened with CFRP. While Fernando Dilum et al. [10], [11] have investigated the end bearing strength of steel RHS that strengthened with CFRP. The structural performance of tubular steel elements strengthened with various layer orientations of CFRP, has been explored in both ways experimentally and numerically by Kabir et al. [12]. Since the bond between CFRP and steel surfaces is one of the important issues in strengthening steel elements using CFRP, Hollaway et al. [13] put the light on some steel surface-CFRP bond difficulties and introduced some recommendations to resolve such adhesion difficulties.

## II. Finding Available Experimental results

One of the finding experimental program in the literature, was that conducted by Tao Chen et al. [14]. The evaluation of the ultimate strength of RHS cracked steel beams strengthened with CFRP, was one of the main objectives of the conducted experimental research. Three of eight conducted tests are described here to be used for the validation of the FE modelling. The authors referred to these three specimens as RHS-II-03-P0, RHS-II-06-P0, and RHS-II-30-P0 to point to the specimens with initial vertical cut depth of 3mm, 6mm, and 30mm respectively. A test of three-point load was designed to be applied to 600 mm effective simple span RHS steel beam with various artificial initial crack depths. The tested beams' cross section is RHS, 100×50×6 mm. The bottom flange was cut at mid span using a saw to create the initial designed cracks. The bottom flange of the prepared RHS steel beams was cut considering three different crack depth values namely 3mm, 6mm, and 30mm respectively to represent various levels of beam damage. The initial cracked beams were strengthened using 1.4 mm thickness CFRP plate. 50 mm width and 400 mm length CFRP plate was agglutinated to the bottom surface of RHS bottom flange using two mixed parts epoxy material. The prepared specimens were loaded at the top middle point till failure using a hydraulic jack of 500 kN capacity. Figure (1) shows the geometry and the cross section of the prepared specimens while Figure (2) shows the setup of the used test rig.

A kind of anchor system was used with the two tested specimens RHS-II-06-P0 and RHS-II-30-P0 to disallow de-bonding of bonded CFRP plates. The end of the CFRP plate was clamped to the steel beam by means of two typical steel plates fastened to the steel beam with four bolts. The results of the experimental tests indicated that, crack has grown through the initial vertical cut on increasing the applied vertical load. It has been declared that, the yielding of cracked zone at the RHS beam mid-span was the controlling mode of failure. Figure (3) pictured the failure patterns of the tested specimens RHS-II-03-P0 and RHS-II-30-P0.

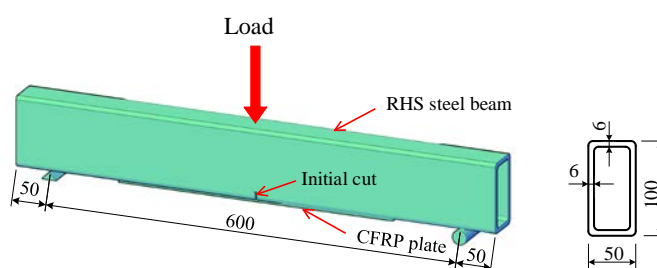


**Figure 1:** Layout and cross section of the tested specimens [14]

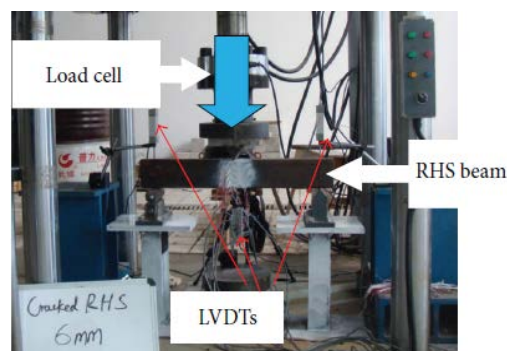
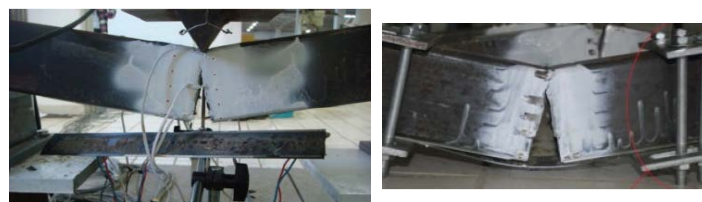


**Figure 2:** Setup of the test rig [14]



RHS-II-03-P0 specimen

RHS-II-30-P0 specimen

**Figure 3:** Failure mode for two of the tested specimens [14]

### III. FINITE ELEMENT MODELLING

The FE model was developed using ABAQUS software. Various geometries and analysis types can be precisely simulated using the wide range of elements library provided by ABAQUS program. The FE models were created to represent the specimens tested in the acquired literature [14].

#### A. Types of Used Elements and Mesh Discretization

In the current study, RHS steel beam was modelled using 3D, 8-node linear solid element, hybrid with constant pressure (C3D8H). CFRP plate was modelled using continuum shell element (SC8R) which allows for capturing deformations and shear stress through its thickness. While 8-node cohesive element (COHD8) was used to represent the adhesive layer. Adhesive layer was connected to adherent parts using surface-to-surface tie contacts. Connecting the adhesive layer to both of the bottom surface of RHS beam and CFRP plate through tie contact option in ABAQUS, enhanced the model since the mesh of the adhesive layer could be independent from the mesh of the adherent parts. In addition to the applied tie contact option between the adhesive layer and the adhered parts, and only on modeling the two tested specimens namely, RHS-II-06-P0 and RHS-II-30-P0, a number of elastic spring elements were used to connect two ends of CFRP plate directly to the bottom surface of RHS steel beam. The spring element (SPRING2) available in ABAQUS that connects two nodes and acts in a fixed direction, was utilized to connect two ends of CFRP plate and RHS beam. Element (SPRING2) can control the relative displacements or rotations between two nodes in assigned directions.

The mesh of RHS steel beam was created where the mesh intensity at mid span is finer than that of the rest of the beam to be able to capture accurately the high stresses developed at this beam zone. Figure (4) shows the geometry of the developed FE model and the varying distribution of the mesh size along the span of the steel beam.

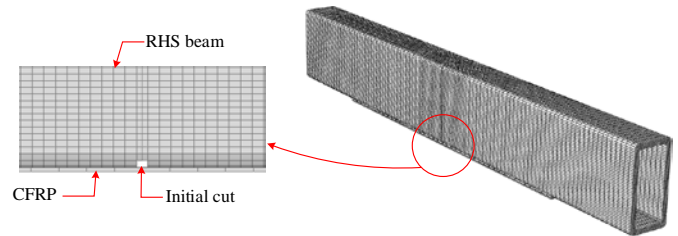


**Figure 4:** Mesh distribution of the FE model

#### B. Boundary Conditions and Applied Load

At the outer bottom surface of simulated RHS beam, two lines of nodes through the beam transversal direction were selected to represent the tested beam supports. The nodes group on the left-hand side were restrained in the three available translations degrees of freedom while the nodes group on the right-hand side were restrained only the vertical direction. The load was applied incrementally to a reference node at mid-span top surface using the displacement control option. To avoid analysis early termination due to stresses concentration at the point of the load application, a rigid part was created using a rigid body option which constrains the displacements of a selected group of elements to that of the reference node.

#### C. Material properties

The material properties reported in the experimental program [14] were used in defining the constitutive material models in the FE analysis. The elastic-plastic model with isotropic strain-hardening available in ABAQUS was used to simulate the material response of both of RHS steel beam and CFRP laminates. In the elastic range, modulus of elasticity  $E$  was taken as  $1.87 \times 10^5$  MPa and  $1.91 \times 10^5$  MPa assigned for RHS beam and CFRP laminates respectively with Poisson's ratio of 0.3 for both of the beam and CFRP respectively. While in the plastic range, the yield stress and the ultimate strength of the steel beam were taken as 298 MPa and 368 MPa respectively. The ultimate strength of 3089 MPa was assigned for CFRP plate while the yield stress was assumed as 2500 MPa since such yield value has not been reported in the experimental program [14].

The traction-separation constitutive law available in ABAQUS [15] was used to model the response of the adhesive material. The traction-separation relation was

assumed to be linear elastic till the damage initiation. The linear relationship is characterized between nominal tractions and nominal strains. Every traction component is assumed to be dependent only on the corresponding nominal strain. The uncoupled traction-separation relationship is given by:

$$\begin{Bmatrix} t_n \\ t_s \\ t_t \end{Bmatrix} = \begin{bmatrix} E_{nn} & & \\ & E_{ss} & \\ & & E_{tt} \end{bmatrix} \begin{Bmatrix} \varepsilon_n \\ \varepsilon_s \\ \varepsilon_t \end{Bmatrix} = E \varepsilon \quad (1)$$

Where

- $t_n$ : nominal traction in the normal direction
- $t_s, t_t$ : nominal tractions in the two local shear directions
- $E_{nn}$ : stiffness in the normal direction
- $E_{ss}, E_{tt}$ : stiffness in the two local shear directions
- $\varepsilon_n$ : strain in the normal direction
- $\varepsilon_{ss}, \varepsilon_{tt}$ : strains in the two local shear directions

As stated earlier, the cohesive element behaves linearly at the starting loading stage. Figure (5) depicts a characteristic traction-separation relationship up to failure since the used notations  $t_n^0, t_s^0, t_t^0$  represent the ultimate values of the nominal stress at the interface normal direction and the two shear directions respectively.  $\delta_n^0, \delta_s^0, \delta_t^0$  represent the effective displacements at the damage initiation.  $\delta_n^f, \delta_s^f, \delta_t^f$  represent the effective displacements at complete damage.

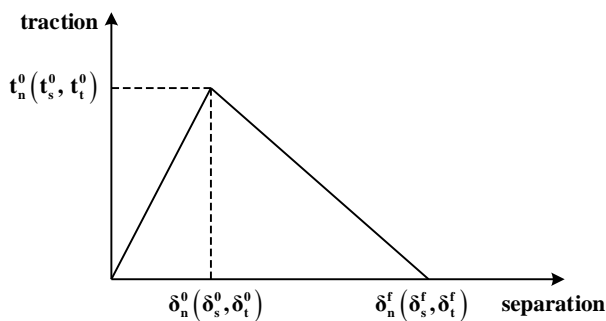


**Figure 5:** Typical traction-separation behavior.

The quadratic interaction equation expressed below is used to determine the damage initiation of the cohesive element.

$$\left\{ \frac{\langle t_n \rangle}{t_n^0} \right\}^2 + \left\{ \frac{t_s}{t_s^0} \right\}^2 + \left\{ \frac{t_t}{t_t^0} \right\}^2 = 1 \quad (2)$$

The deformations of the cohesive element considered in this study are mixed mode deformations that composed of normal and shear deformations. Three magnitude values of mod mix are used in ABAQUS, one is related to tractions and two are related to energies. The following expressions determine the mode-mix relied on energies.

$$m_1 = \frac{G_n}{G_T}, \quad m_2 = \frac{G_s}{G_T}, \quad m_3 = \frac{G_t}{G_T} \quad (3)$$

Where  $G_n, G_s,$  and  $G_t$  are the work done by the traction and their related displacements in the normal direction and in the two shear directions, respectively and  $G_T = G_n + G_s + G_t$ . The other terms defined by the mixed mode related to the components of the traction are  $\phi_1$  and  $\phi_2$  which are given by:

$$\phi_1 = \left( \frac{2}{\pi} \right) \tan^{-1} \left( \frac{\tau}{\langle t_n \rangle} \right), \quad (4)$$

$$\phi_2 = \left( \frac{2}{\pi} \right) \tan^{-1} \left( \frac{t_t}{t_s} \right)$$

since  $\tau$  expresses the effective shear traction,

$$\tau = \sqrt{t_t^2 + t_s^2}.$$

Figure (6) shows the angular measurements employed in the above relations.

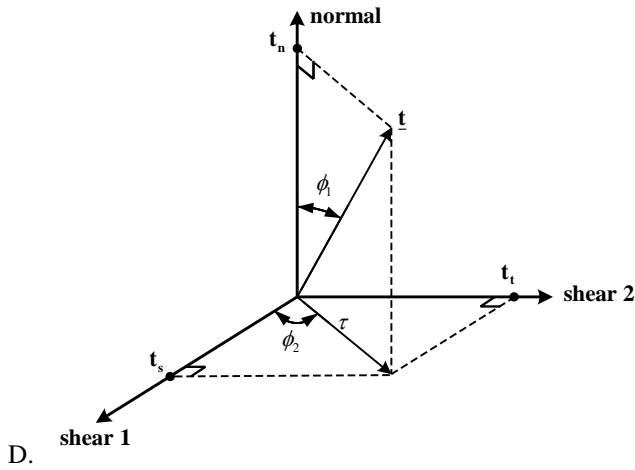


**Figure 6:** Measurements of mixed model relevant to traction

The evolution damage is defined by two terms in ABAQUS. One of two alternatives could be included in the first evolution damage term. The first alternative is the ratio of the effective displacement at complete failure,  $\delta_m^f$ , to the effective displacement at damage initiation,  $\delta_m^0$ . The second alternative is the dissipated energy as a result of failure,  $G^C$  as explained in Figure (7). The second term of the damage evolution, is the variable  $D$  that specifies the damage evolution nature in the range from the damage initiation to complete failure. Such variable,  $D$ , could be introduced to ABAQUS through linear or exponential function or as a tabular function of the ratio of the effective displacement to the damage initiation effective displacement.

By the damage commencement, the law of the damage evolution is utilized to represent the deterioration of the material stiffness. In the current study, the damage evolution is identified using the effective displacement. The values of  $\delta_m^f$  and  $\delta_m^0$  (the effective displacement at complete damage,  $\delta_m^f$ , relative to the effective displacement at damage initiation,  $\delta_m^0$ ) are specified as a tabular function of the mixed mode considering an exponential softening mode as presented in Figure (8). The evolution in the range between the damage initiation and the complete failure is characterized as an exponential function of the effective displacement after damage initiation.

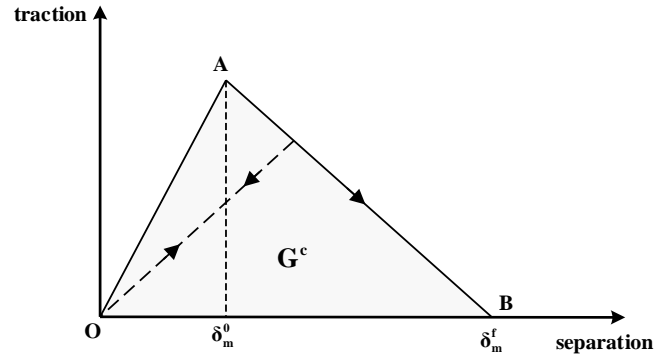


**Figure 7:** Response of traction-separation model.

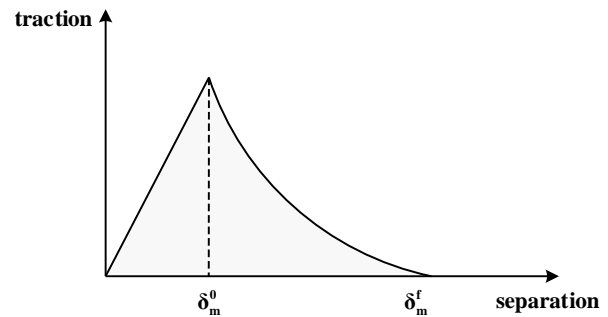


**Figure 8:** Exponential damage evaluation

The damage variable  $D$  is used to specify the damage evolution in the range between the damage initiation and the complete failure. The exponential low shown in Equation [5] is used to define the damage variable  $D$ .

$$D = 1 - \left\{ \frac{\delta_m^0}{\delta_m^{\max}} \right\} \left\{ 1 - \frac{1 - \exp\left(-\alpha \left( \frac{\delta_m^{\max} - \delta_m^0}{\delta_m^f - \delta_m^0} \right)\right)}{1 - \exp(-\alpha)} \right\} \quad (5)$$

where  $\alpha$  is a non-dimensional parameter, defines the damage evolution rate and  $\delta_m^{\max}$  is the maximum effective displacement value achieved during the loading history.

#### IV. VALIDATION OF THE NUMERICAL SIMULATION

The carried-out FE analysis was validated by comparing the numerical results to the corresponding recorded experimental results in the finding literature. The applied load versus the mid-span beam deflection

resulted curves for both FE analysis and experimental tests are compared in the Figures 9, 10, and 11. It is obvious from the compared load-displacement curves that, the behavior of the FE model seems to be stiffer than the tested beam in the early loading stage and that might return to the proposed initial geometric imperfections which may not exactly alike with that existed in the tested specimens. Form table 1, it can be recognized that the variance resulting from the FE analysis in estimating the ultimate load of the strengthened RHS steel beams reaches to 6.94% from that of the corresponding tested specimen. It should be stressed on that, the two obtained large variance values between the results of the FE analysis and that of the experimental tests are related to the simulated FE models of the tested specimens namely, RHS-II-06-P0 and RHS-II-30-P0. The main reason for such relatively high variances is that, on building those two FE models, two ends of CFRP plate were connected to RHS beam via elastic spring elements to simulate the used clamping system that connected the ends of CFRP to the tested specimens. In the numerical simulation, it was a kind of complexity to gather two types of connection as, tie contact option and spring elements at the same elements region. Therefore and to overcome this obstacle, the adhesive layer was removed from those regions at the ends of CFRP plate and the connection there depended only on the assigned spring elements. In this case, it was highly expected that the results of the FE analysis and that of the conducted test results could differentiate since in the FE modeling, a shorter adhesive layer was considered compared to that of the tested specimen. Moreover, uncalibrated elastic spring elements were added to connect ends of CFRP laminates to RHS steel beam.

On the other hand, the conducted comparison between the results of the FE analysis and the carried out test concerning the simulated tested specimen, RHS-II-03-P0, shows a close agreement. In this FE model, the connection between adhesive material and adhered parts depended only on the contact option in simulating the agglutinated CFRP to bottom surface of the tested beam. It can be recognized that the variance resulting from the FE analysis in evaluating the ultimate load of the strengthened steel beam does not overreach 2.0% from that of the tested specimen. Such resulted reasonable small variance in the achieved ultimate loads from the FE analysis and the conducted experimental tests is accepted especially with modelling of such uncertainty

material behavior as adhesive laminates. The numerical simulation presented a robust capability in predicting the ultimate load for the tested RHS steel beam retrofitted and strengthened with epoxy adhered CFRP laminates. It is observed that, the failure mode of the three numerically analyzed strengthened beams is de-bonding of CFRP plate that triggered close to the beam mid-span. The failure pattern of de-bonding of CFRP laminates, was recognized in the numerical analysis by commencing of adhesive layer demolition after achieving ultimate strength load. Figure (12) pictures Mises stresses for both of steel beam and CFRP plate at the ultimate strength load for RHS-II-03-P0 analyzed specimen. Because of the obtained reasonable results, the FE model simulated the tested specimen RHS-II-03-P0 was used in the conducted parametric study presented in the following section.

TABLE I

ULTIMATE LOADS ACHIEVED FROM THE EXPERIMENTAL TESTS AND FE ANALYSIS

Specimen	Initial cut depth (mm)	Ultimate load (kN)		$\frac{P_{u(FE)} - P_{u(test)}}{P_{u(test)}} \%$
		$P_{u(test)}$	$P_{u(FE)}$	
RHS-II-30-P0	30	72.5	67.47	-6.94
RHS-II-06-P0	6	102.8	99.52	-3.19
RHS-II-03-P0	3	110.6	112.8	2.0

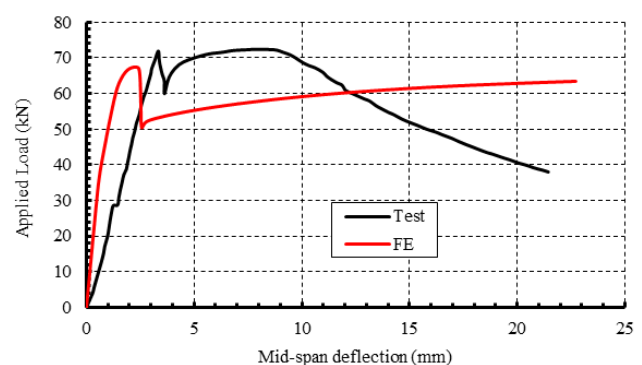
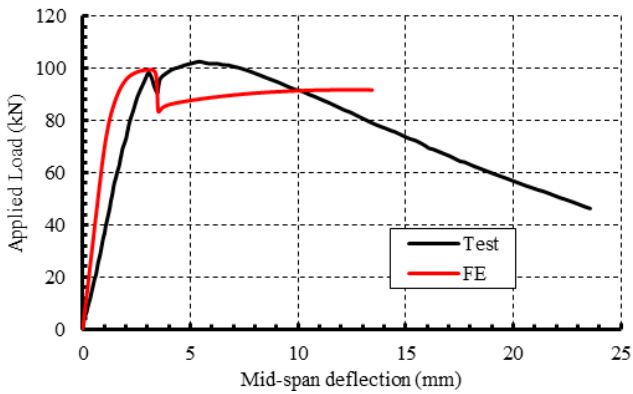
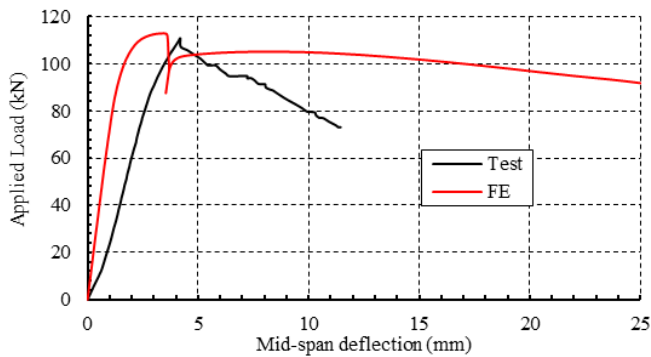


Figure 9: Comparison of load-deflection curves resulted from experimental test and FE analysis for specimen RHS-II-30-P0



**Figure 10:** Comparison of load-deflection curves resulted from experimental test and FE analysis for specimen RHS-II-06-P0



**Figure 11:** Comparison of load-deflection curves resulted from experimental test and FE analysis for specimen RHS-II-06-P0

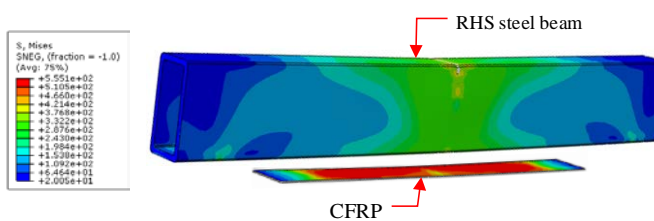


**Figure 12:** Misses stress distribution at the ultimate strength for simulated specimen RHS-II-03-P0

## V. PARAMETRIC STUDY

The strength of rehabilitated and strengthened RHS steel beams could be improved by adapting some parameter such as the length of the adhesive layer between the steel beam and CFRP, the thickness of the adhesive layer, and the type of the employed adhesive material. In the following subsections, a kind of parametric study was conducted to highlight the effect of the aforementioned parameters in the strengthened beam ultimate strength. The developed FE model that

employed to simulate the tested specimen RHS-II-03-P0, was used in the carried out parametric analyses to investigate the parameters that may improve the functionality of the epoxy adhesive layer in bonding CFRP laminates to the steel beam bottom surface.

### A. length of Adhesive Layer

The length of the adhesive layer in all experimentally tested specimens [14], is equal to length of CFRP plate of 440 mm. In the current parametric analysis, more four lengths of adhesive layer are considered namely, 585 mm, 380 mm, 308 mm, and 104 mm respectively. It is observed that, the ultimate strength of strengthened beam has not been altered for the used adhesive layer of lengths 580 mm, 440, and 380 mm. in the opposite, the strength of the analyzed beams has been degraded with the used adhesive layer of lengths 308 mm and 104 mm length as presented in Figures (13, 14). In can be observed that, the adhesive layer length of 380 mm is the optimum length of the adhesive layer that could be employed to achieve the maximum strength for such RHS steel beam strengthened with CFRP plate.

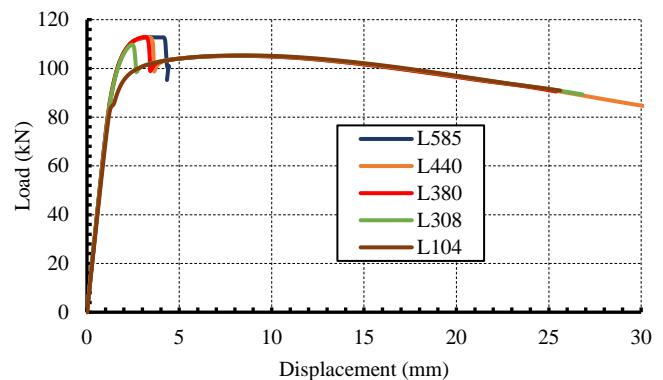


**Figure 13:** Mid-span load-deflection curves for various lengths of adhesive

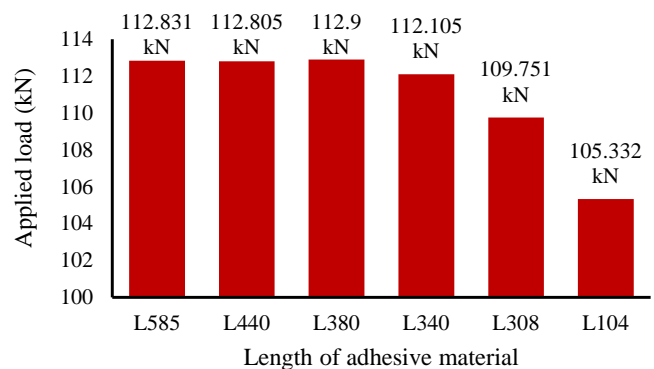


**Figure 14:** Strengthened beam ultimate load strength for various lengths of adhesive

## B. Thickness of adhesive layer

The thickness of the used adhesive layer may affect the strength of the rehabilitated steel beams. Therefore, the current parametric study is focused on the thickness of the adhesive layer that bonds CFRP laminate to the bottom surface of the steel beams. Three different thickness were considered in the current analysis namely, 0.2mm, 0.4mm, and 0.6mm respectively.

According to the previous parametric study, a length of 380 mm adhesive layer was chosen to be applied in the current parametric study. Figure (15) shows the mid-span load-displacement curves for the three analyzed FE models with different values of adhesive layer thickness. It is obvious that, on increasing the thickness of adhesive layer, the ultimate strength increases as depicted in Figure (16). More analyses are required to determine the optimum adhesive layer thickness and also to check the effect of adhesive layer thickness on more parameters such as the elastic stiffness and the ductility that could be reached before failure.

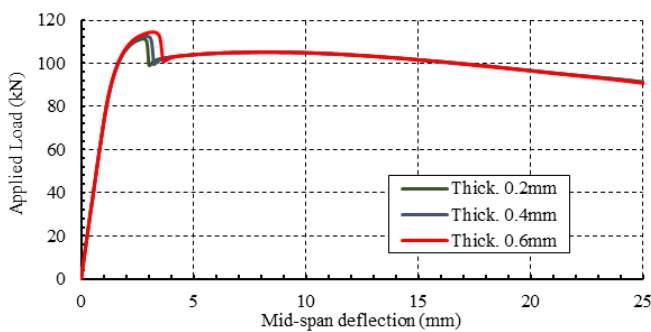


**Figure 15:** Mid-span load-deflection curves for various thickness values of adhesive layer

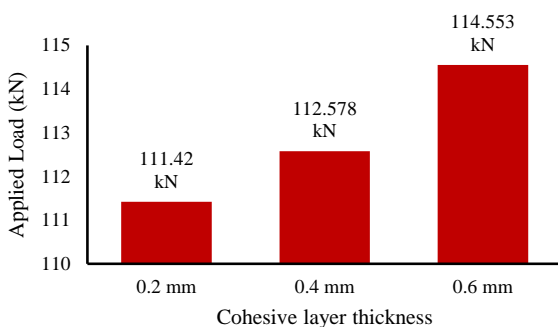


**Figure 16:** Strengthened beam ultimate load strength for various thickness values of adhesive layer

## C. Type of Adhesive Material

The type of the adhesive material may influence the behavior of the strengthened steel beam with CFRP

laminates. Therefore, a parametric study was conducted to investigate the effect of the type of the adhesive material on the strengthened steel beam. Three types of adhesive materials available in [12] namely, MBrace saturant, Araldite K630, and Sikadur 330, were used in three different FE models. Figure (17) shows the achieved ultimate strength related to each used type of adhesive material. Regarding the considered case of strengthening a cracked RHS beam, the adhesive material with properties of less stiffness and higher tensile and shear strength, MBrace saturant compared to the other two material types, demonstrated a better performance in strengthening RHS cracked beams. It is obvious from the comparison presented in Figure (17) that, the use of MBrace saturant adhesive material results in a greater obtained beam ultimate strength.

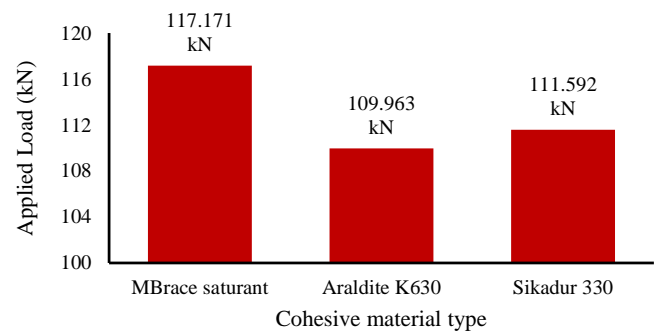


**Figure 17:** Strengthened beam ultimate load strength for various material types of adhesive layer

## VI. CONCLUSION

In this study, the behavior of RHS steel beams strengthened with CFRP is numerically investigated. The developed FE model is validated with the experimental tests conducted by [14]. The current study is concentrated on the CFRP only adhered to the outer surface of initially cracked RHS beams without any end external clamping or pre-stressing to CFRP plate. The conducted comparison between the experimentally tested RHS steel beam with 3mm depth initially cracked and that of numerically simulated demonstrated a close agreement in the terms of mid-span load-displacement curve and in the failure type. In this FE model and after achieving the ultimate strength, the beam resistance was degraded because of the de-bonding of CFRP plate due the demolishing of the adhesive material. The failure of the adhesive material was indicated in the FE model with zero stress zones through the adhesive layer.

The failure type of both experimentally and numerically analyzed strengthened RHS beams, is a kind of adhesive material failure that issued de-bonding of CFRP plate and a total beam failure. Therefore a sort of parametric studies were conducted to investigate the effect of certain parameters of the adhesive material on the maximum strength could be achieved before the failure of the strengthened RHS steel beam. The conducted analysis indicated that, 380 mm adhesive layer length is sufficient to allow the strengthened RHS beam to reach the maximum strength. It is observed that, any further increasing in the length of the bond surface, did not gain any more load strength. It could be recommended that, the economic length of the adhesive layer is about 8 times the strengthened beam width.

The carried out parametric analysis demonstrated that, increasing the thickness of the adhesive layer results in increasing the ultimate strength of the strengthened beam. Additional parametric analysis considering the thickness of the adhesive layer parameter, could add more lights in determination the optimum thickness of the adhesive layer that could achieve maximum beam resistance load. Based on the last conducted parametric analysis, the type of the adhesive material, may control the strengthened beam ultimate strength. It is observed that, the adhesive material with low elastic stiffness and higher tensile strength is able to attain higher strengthened beam load resistance comparable to the use of adhesive material of varying properties.

## VII. REFERENCES

- [1] Kambiz N., N. H. Ramli S., Mohd Z. J., "Flexural Strengthening of Steel I-beams by using CFRP Strips" *International Journal of the Physical Sciences* Vol. 6(7), pp. 1620-1627, 4 April, 2011.
- [2] Kambiz N., N. H. Ramli S., Mohd Z. J., "Failure Analysis and Structural Behaviour of CFRP Strengthened Steel I-beams" *Journal of Construction and Building Materials*, Vol. (30), pp. 1-9, 2012.
- [3] Mohammed A., Lee C., Martin G., "CFRP Strengthening of Steel Beams with Web Openings" *Proceedings of Structural Faults & Repair 2016: 16th International Conference*. ed. / M C Forde. Edinburgh, 2016. 1754.
- [4] Hongyuan T., Canjun W., Ruijiao W., "Enhancing Stability of Thin-Walled Short Steel Channel Using CFRP under Eccentric Compression" *International Journal of Polymer Science*, Vol. 2016, Article ID 2790385, 11 pages, 2016.
- [5] Jiao H., Zhao X. L., "CFRP Strengthened Butt-Welded Very High Strength (VHS) Circular Steel tubes" *Journal of Thin-Walled Structures*, Vol. 42, pp. 963-978, 2004.
- [6] Fawzia S., Al-Mahaidi R., Zhao X.L., Rizkalla S., "Strengthening of Circular Hollow Steel Tubular Sections Using High Modulus CFRP Sheets" *Journal of Construction and Building Materials*, Vol. 21, pp. 839-845, 2007.
- [7] Haedir J., Zhao X. L., "Flexural and Axial Behaviour of CFRP Strengthened Steel Circular Hollow Section Beams and Short Columns" *Proceeding of Annual Stability Research Council Grapevine, Texas*, April 18-21, 2012.
- [8] Shanmugavalli B., Sundarraja M.C., "Behaviour of CHS Short Columns Strengthened with CFRP Composites under Axial Compression" *IOSR Journal of Mechanical and Civil Engineering*, Vol. 2, pp. 59-66, 2014.
- [9] Xiao-Ling Z., Dilum F., Riadh A., "CFRP Strengthened RHS Subjected to Transverse and Bearing Force" *Journal of Engineering Structures*, Vol. 28, pp. 1555-1565, 2006.
- [10] Fernando D., Yu T., Teng J. G., Zhao X. L., "CFRP Strengthening of Rectangular Steel Tubes Subjected to End Bearing Loads: Effect of Adhesive Properties and Finite Element Modelling" *Journal of Thin-Walled Structures*, Vol. 47, pp. 1020-1028, 2009.
- [11] Fernando D., Yu T., Teng J. G., "Finite Element Analysis of Debonding Failures in CFRP-Strengthened Rectangular Steel Tubes Subjected to an End Bearing Load" *6th International Conference on FRP Composite in Civil Engineering*, pp. 1-8, 2012.
- [12] Kabir M.H., Fawzia S., Chan T.H.T., Gamage J.C.P.H., Bai J.B., "Experimental and Numerical Investigation of the Behaviour of CFRP Strengthened CHS beams Subjected to Bending" *Journal of Engineering Structures*, Vol. 113, pp. 160-173, 2016.
- [13] Hollaway L. C., Zhang L., Photiou N. K., Teng J. G., Zhang S. S., "Advances in Adhesive Joining of Carbon Fibre/Polymer Composites to Steel Members for Repair and Rehabilitation of Bridge Structures." *Adv. Struct. Eng.*, 9, pp. 791-803, (2006).
- [14] Tao C., Ming Q., Xiang-Lin G., Qian-Qian Y., "Flexural Strength of Carbon Fiber Reinforced Polymer Repaired Cracked Rectangular Hollow Section Steel Beams" *International Journal of Polymer Science*, Volume 2015, Article ID 204861, 9 pages, 2015.
- [15] Hibbitt, Karlson, Sorenson, "ABAQUS User's Manual" Version 6.14, Part 1&2, 2014.